AMD-Vol. 174/FED-Vol. 175, Fluid Mechanics Phenomena
in Microgravity
ASME 1993

COMPUTATIONAL INVESTIGATION OF THERMAL MIGRATION OF BUBBLES AND DROPS

Selman Nas
Department of Aerospace Engineering

Grétar Tryggvason*
Department of Mechanical Engineering
and Applied Mechanics

University of Michigan
Ann Arbor, Michigan

ABSTRACT

Numerical simulations of two-dimensional bubbles moving in a nonuniform temperature field are presented. The full Navier-Stokes equations as well as the energy equation for the temperature distribution, are solved for the fluid inside and outside of the bubbles by a Front Tracking/Finite-Difference Method. The material properties of the bubble fluid and the ambient fluid are different, and we assume temperature dependent surface tension. We explore the dependence of the thermal migration velocity and the deformation on the various nondimensional parameters. The interaction of two bubbles is then explored. The bubbles line up across the channel and move side by side toward the hotter wall. Similar evolution is seen for six bubbles. The bubbles move in two layers—one consisting of four bubbles and the other one of two—that migrate toward the hot wall with different velocity. Although the bubbles strive to line up in the direction perpendicular to the temperature gradient, they generally place them self as far away from each other as possible, along this line.

INTRODUCTION

Bubbles and drops in an ambient fluid which has a temperature gradient will move toward the hot region due to thermocapillary forces. Surface tension decreases with increasing temperature and the nonuniform surface tension along the bubble surface causes shear stresses that are transmitted to the outer fluid by viscous forces, thus inducing a motion of the bubble in the direction of thermal gradient. In space, where buoyancy forces are negligible, thermocapillary forces can be dominant. For material processing in microgravity, thermal migration can be used, for example, to remove gasses in melts before solidification. Thermocapillary migration can also be important in the design of two-phase heat exchanger in space. Accumulation of bubbles on heated surfaces may act like an insulator and preventing heat transfer to the surface. To understand the interaction of many bubbles in thermocapillary induced motion and to investigate the effect of the various governing parameters, we solve the full Navier-Stokes equations and the energy equation for both fluids, computationally.

Thermal migration of bubbles was first examined by Young et al. (1959), both theoretically and experimentally. Young et al. were able to hold a buoyant bubble stationary by applying a downward temperature gradient and gave a first order approximation to the terminal velocity in the limit of negligible convective transport of momentum and energy with the assumption that the bubble maintains its spherical shape. They also verified that the temperature gradient required to hold a bubble stationary increased with bubble radius and that this gradient is independent of viscousity as predicted by their theoretical model. Later, Subramanian (1981) obtained the solution for small but nonzero convective heat transfer by using asymptotic expansion technique. Merrit (1988) extended the theory of Young et al. to include gravity. Balasubramaniam and Lavery (1989), for

*Also: Institute for Computational Mechanics in Propulsion, Lewis Research Center, Cleveland, OH 44135

a large range of nondimensional numbers, numerically solved the problem for an isolated axisymmetric spherical bubble. They found that the scaled bubble velocity is more sensitive to the Marangoni number at a fixed Reynolds number than to Reynolds number at a fixed Marangoni number. Balasubramaniam and Chai (1987) have given an exact solution for small Marangoni number for a single bubble. They also computed the small deformation from a sphere shape. Chen and Lee (1992) investigated numerically the effect of surface deformation on terminal velocity of a single bubble and concluded that surface deformation reduces the terminal velocity considerably. Experimental results are given by Merrit et al. (1988) and Thompson (1979) for bubbles and by Barton and Subramanian (1989), Rashidna and Balasubramaniam (1989) and Wozniak and Siekman (1989) for liquid drops. Others have examined the problem for two bubbles or drops, but limited to either small Marangoni or Reynolds number. Meyyapan at al. (1983) analyzed the motion of two bubbles oriented arbitrarily with respect to the temperature gradient, using an approximate method. They found that each bubble moves with the same velocity that it has if it is isolated. Same case for drops was analyzed by Anderson (1985) who also predicted the migration velocity of a cloud of equal sized drops. Recently, Strape (1992) analytically examined the interaction of bubbles in the zero Marangoni and Reynolds number case. He also assumed that the Capillary number is negligible so that the bubbles are always spherical. He has given the trajectories for two bubble in these limits. He also found that for a statistically homogeneous cloud of bubbles, the bubble collision rate increases with the standard deviation of the bubble size distribution.

The interaction of bubbles and drops with plane surfaces is the subject of other investigations. Ascoli and Leal (1990) considered the thermocapillary migration of a deformable drop moving normal to a planar wall and found that the deformation increases with increasing effective Capillary number. A gas bubble interacting with a planar wall was studied by Meyyapan and Subramanian (1987).

The literature is more rich for single bubbles or drops than the interaction of many bubbles and drops. In most of the work, it was assumed that the bubbles do not deform and that convective transfer can be neglected. Here we present results for one and many bubbles by solving the full governing equations numerically in two dimension. In our computations, we do not impose any condition on the shape of the bubbles, although we find that the bubbles remain nearly spherical in most cases.

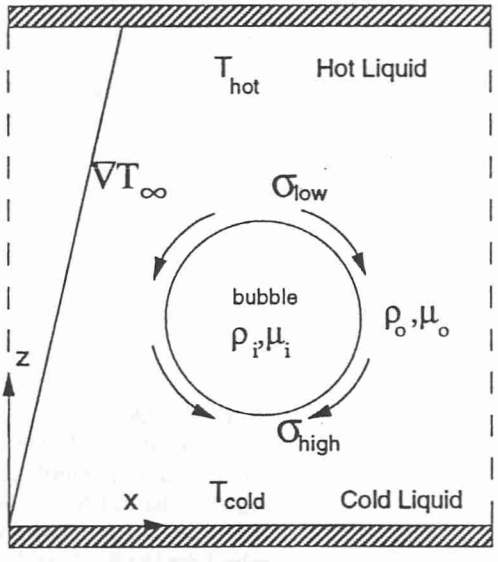

Figure 1: THE COMPUTATIONAL SETUP. THE TWO-DIMENSIONAL DOMAIN IS RESOLVED BY A REGULAR GRID.

FORMULATION & NUMERICAL METHOD

The physical problem and the computational domain is sketched in Figure 1. We have a wall bounded region in the z direction and the domain is periodic in the x direction. The bubble has constant physical properties denoted by the subscript i and the ambient fluid has properties denoted by the subscript o. The top wall is hot and the bottom wall is cold. The surface tension varies along the interface. Initially, the temperature is linearly increasing in the z direction and we expect that the bubble will move towards the hotter wall.

The Navier-Stokes equations are valid for both fluids, and a single set of equations can be written for the whole domain as long as the jump in viscosity and density is correctly accounted for and surface tension is included. Here we treat the surface tension forces as body forces and write only one equation for the whole domain. The Navier-Stokes equations can be written in conservative form as follows,

$$\frac{\partial \rho \bar{u}}{\partial t} + \nabla(\rho \bar{u}^2) = -\nabla p + \nabla \cdot \mu(\nabla \bar{u} + \nabla \bar{u}^T) + \delta(\bar{x} - \bar{x}_f)(\sigma \kappa \hat{n} + \frac{\partial \sigma}{\partial s}\hat{s}) \quad (1)$$

In the last term, we include the surface tension forces acting on the interface by a delta function. Here $\bar{x}$ is

the velocity field, ρ is the density, p is the pressure, μ is the viscosity, σ is the surface tension, κ is the mean curvature and $\bar{x}_f$ is the position of the interface.

The energy equation can be written as

$$\rho c_p \left(\frac{\partial T}{\partial t} + \nabla \cdot (\bar{u} T) \right) = \nabla \cdot (k \nabla T), \qquad (2)$$

where T is the temperature and k and c_p are the coefficients of heat conduction and heat capacity, respectively. Both fluids are immiscible and the physical properties are constant in each fluid. Therefore, the equations of state for density, viscosity, heat capacity and heat conduction are

$$\frac{D\rho}{Dt} = 0; \qquad \frac{D\mu}{Dt} = 0 \qquad (3a)$$

$$\frac{Dk}{Dt} = 0; \qquad \frac{Dc_p}{Dt} = 0. \qquad (3b)$$

The incompressibility constrain gives the divergence free velocity field condition as

$$\nabla \cdot \bar{u} = 0. \qquad (4)$$

If we combine the momentum equation and the incompressibility condition, this leads to a non-separable elliptic equation for the pressure. Since the physical properties are taken to be constant, density field is independent of temperature variation and we have excluded natural convection in this problem.

We take the surface tension to be a linear decreasing function of the temperature:

$$\sigma = \sigma_o + \sigma_T (T_o - T) \qquad (5)$$

where

$$\sigma_T = -(d\sigma/dT) = \text{constant}$$

and σ_o is the average surface tension at a reference temperature T_o. In many cases, σ_T can be assumed to be a constant and for simplicity we assumed that it is so here. σ_T is positive for all fluids, so increasing temperature reduces the surface tension. In a nonuniform temperature gradient, the cold side of the bubble will have a higher surface tension than the warm side and it will therefore pull surface from the warm side, where surface will be generated, around the bubble to the cold en, where the surface will disappear. This movement of the surface, with its viscous drag upon the outer fluid, will pick up a sheet of liquid and jet it off the cold back end. By jetting liquid one way, the bubble propels itself up the temperature gradient. Thermodynamically, such a self-propelling bubble is a heat engine. Whenever surface is created, heat is absorbed, and whenever surface is destroyed heat is given off. Therefore a swimming bubble absorbs heat at its hot end and rejects heat at its cold end (Trefethen, 1963).

The numerical technique used for the simulations presented in this paper is the Immersed Front Tracking method for multi-fluid flows developed by Unverdi (1990) and discussed by Unverdi and Tryggvason (1992 a,b). To solve the Navier Stokes equations we use a fixed, regular, staggered grid and discretize the momentum equations using a conservative, second order centered difference scheme for the spatial variables and an explicit first order time integration method. We have used second order time integration in other problems and generally find little differences for relatively short simulations times as those of interest here. The effect does show up in long time simulations and is usually accompanied by a failure to conserve mass. In the computations discussed here, mass is always conserved within a fraction of a percent. The interface is represented by separate computational points that are moved by interpolating their velocity from the grid. These points are connected to form a front that is used to keep the density and viscosity stratification sharp and to calculate surface tension forces. At each time step information must be passed between the front and the stationary grid. This is done by a method that has become known as the Immersed Boundary Technique and is based on assigning the information carried by the front to the nearest grid points. While this replaces the sharp interface by a slightly smoother grid interface, all numerical diffusion is eliminated since the grid-field is reconstructed at each step.

The original Immersed Boundary Technique was developed by Peskin and collaborators (see e.g. Peskin 1977) for homogeneous flows. The extension to stratified flows includes a number of additional complications. The first is that density now depends on the position of the interface and has to be updated at each time step. There are several ways to do this but we use a variant of the method developed by Unverdi (1990) where the density jump at the interface is distributed onto the fixed grid to generate a grid-density-gradient field. The divergence of this field is equal to the Laplacian of the density field and the resulting Poission equation can be solved efficiently by a Fast Poisson Solver. The particular attraction of this methods is that close interfaces can interact in a very natural way, since the grid-density gradients simply cancel. Therefore, when two interfaces come close together the full influence of the surface tension forces from both interfaces is in-

cluded in the momentum equations, but the mass of the fluids in the thin layer between the interfaces—which is very small—is neglected. A second complication is that the pressure equation now has a nonconstant coefficient (or is non-separable) since the density varies. This prevents the use of Fast Poisson Solvers based on Fourier Methods, or variants there of, and we have used red and black SOR.

The computation of the surface tension forces poses yet another difficulty. Generally, curvature is very sensitive to minor irregularity in the interface shape and it is difficult to achieve accuracy and robustness at the same time. However, by computing the surface tension forces directly by

$$F_s = \int \frac{\partial \sigma s}{\partial s} ds.$$

we ensure that the net surface tension force is zero, or:

$$\oint \sigma \kappa \mathbf{n} da = 0.$$

Here, $\mathbf{n}$ is the outward normal and κ is the mean curvature. This is important for long time simulations since even small errors can lead to a net force that moves the bubble in an unphysical way.

The energy equation is solved in the same way as the momentum equation. The temperature on the front is interpolated from the neighboring stationary grid points by using an interpolation function invented by Peskin (1977). Given the temperature, surface tension can be found and the surface forces computed. The momentum and the energy equations are coupled through this relation.

Following other investigators we present our results in nondimensional variables. The flow is governed by

$$a,\ \sigma_o,\ \mu_o,\ \rho_o,\ c_{po},\ k_o,\ \mu_i,\ \rho_i,\ c_{pi},\ k_i,\ \sigma_T,\ \nabla T_\infty.$$

Here a is the typical bubble radius and ∇T_∞ is the undisturbed temperature gradient in the ambient fluid far from the bubble. This leads to the following nondimensional numbers;

$$\frac{\rho_i}{\rho_o},\ \frac{\mu_i}{\mu_o},\ \frac{c_{pi}}{c_{po}},\ \frac{k_i}{k_o},\ Ma = \frac{\sigma_T a^2}{\mu_o \alpha_o} \nabla T_\infty,$$

$$Re = \frac{\sigma_T \rho_o a^2}{\mu_o^2} \nabla T_\infty,\ Ca = \frac{\sigma_T a}{\sigma_o} \nabla T_\infty$$

where,

$$\alpha_o = \frac{k_o}{\rho_o c_{po}}$$

Here Ma is the Marangoni number, Re is the Reynolds number and Ca is the Capillary number. These three nondimensional numbers are based on the properties of the outer fluid. Sometimes the Prandtl number, $Pr_o = \nu_o/\alpha_o$, can also be used instead of the Re number. α_o is the thermal diffusivity for the outer fluid. As it is usually done in the literature for Marangoni bubble motion, we define a reference velocity as

$$U_r = \frac{\sigma_T a}{\mu_o} \nabla T_\infty.$$

The nondimensional numbers can now be written in a much simpler form:

$$Ma = \frac{U_r a}{\alpha_o}, \qquad Re = \frac{U_r a}{\nu_o}, \qquad Ca = \frac{\mu_o U_r}{\sigma_o}$$

The Marangoni number is the Péclet number as it is usually used in heat transfer phenomena and is the product of the Prandtl and the Reynolds number. The velocities are scaled by the reference velocity defined above. Time is scaled by the ratio of initial bubble radius and the reference velocity.

When the nondimensional numbers are either small or large, several interesting limiting cases arise. In the zero Marangoni number limit the energy equation duces to the Laplace equation for temperature since the convective transport of energy can be neglected in this case. Hence, the problem becomes a quasi-static problem. For a gas bubble, when the physical properties of the gas are much smaller then of the ambient fluid, the energy transfer on the bubble surface can be neglected. This implies that the isolines for temperature should be perpendicular to the bubble surface. Small Prandtl number results apply to liquid metals and large Prandtl number to heavy oils. Liquids have Prandtl number on the order of 1. Typical values are Pr=7 for water and Pr=0.72 for air, under standard condition. The zero Reynolds number limit reduces the momentum equation to the steady case since the inertial affects can be neglected in this limit.

When the Marangoni number is large, the convective terms in the energy equation are dominant. In this limit, conduction of the energy can be neglected. This is the case where unsteadiness comes into effect. If Reynolds number is of the order of unity, large Prandtl number is the reason for high Marangoni number. Heavy oils like silicon oil have high Prandtl number of the order of 10^3 or 10^4.

In the limit of zero Capillary number, it can be assumed that the deformation from a spherical shape are negligible. As the Capillary number increases, deformation increase. As the deformation from a spherical shape is high, the scaled terminal velocity of t

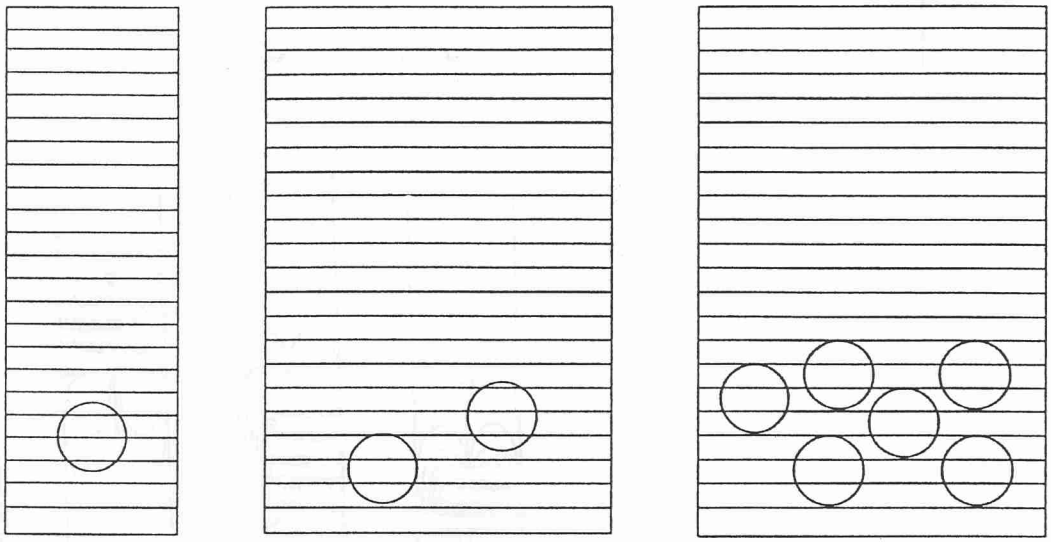

Figure 2: THE INITIAL CONDITIONS FOR ONE, TWO AND SIX BUBBLE COMPUTATIONS.

bubble/drop decreases. In the zero Capillary and Marangoni number limit, the scaled rise velocity is known to be 0.5. In our calculations, where Ca = 0.0166, the scaled rise velocity for all the single bubble cases is in good agreement with the results of Chen and Lee (1992).

In our simulations we include all terms in the governing equations and do not impose any restrictions inherent for these limiting cases.

RESULTS AND DISCUSSIONS

First we compute the motion of a single bubble. We have explored the sensitivity of the solution to the grid resolution by simulating a single bubble on a 32×32, 40×40, 50×50 and 64×64 for a square domain which is five bubble radius in each direction. As we increase the resolution the trajectories and the terminal velocities converge and we observed that beyond the 50×50 grid the change is negligible. The test covered the range of parameters simulated here, but we note that different governing parameters generally require different resolution for convergence.

Figure 2 shows the initial placement of the bubbles for the computations presented in this paper. In 2a we follow the rise of a single bubble. The size of domain in horizontal direction is 2.5 times larger than the bubble diameter and the vertical size of the domain is 15 times larger than the bubble diameter. The bubble is placed far enough from the lower wall so that boundary effects should not influence the bubble motion. Upon release of the bubble, we observed that for a short period, the bubble deforms and its shape oscillates. The oscillation in shape die out as the bubble moves towards the hot wall. At later times, we did not see any significant deformation from a cylindrical shape. In all these calculation, the Capillary number is fixed with $Ca = 0.0166$. Unless noted otherwise, all other nondimensional numbers are as in Figure 5b. Figure 3 shows the temperature and stream function contours at different nondimensional times. Stream function contours clearly show the dividing streamline and a stagnation point behind the bubble. Here, we plot the stream function contours in a laboratory fixed frame. The contours in a frame which is moving with the bubble does not show any interesting behavior. The streamlines shown here are nearly identical to those shown by Subramanian (1992) for axisymmetric bubbles. The rise velocity of the bubble is shown in Figure 4. The first period is the impulsive movement of the bubble. Then the bubble slows down and reached a steady state rise. It continues to rise with this terminal velocity until it reaches to the upper wall. Although we terminate these computations before the bubble reaches the top of the domain, we have conducted other calculation where the bubble interacts with the wall and found deformation similar to those computed by Ascoli and Leal (1990).

To show the effect of the various nondimensional parameters we show, in Figure 5, the temperature and

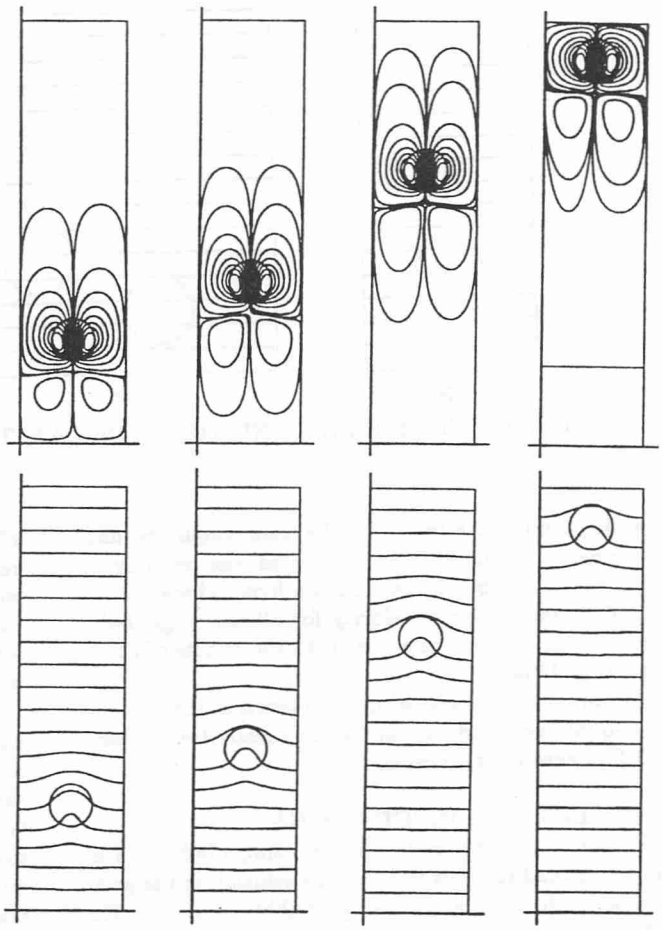

Figure 3: TEMPERATURE CONTOURS (BOTTOM) AND STREAMLINES (TOP) FOR THE SINGLE BUBBLE IN FIGURE 2a. THE NONDIMENSIONAL TIME, t*, IS EQUAL TO 12.5, 37.5, 87.5, 137.5.

stream function contours for several different cases. In all frames, the bubble has reached an essentially steady state and we only show the contours close to the bubble. The bubble remains cylindrical for the computations shown here and the major difference is the shape of the temperature contours and the structure of the wake. As the bubbles rise they carry cold fluid from the bottom. This fluid heats up as the bubble moves into warmer fluid and the disturbance in the temperature contours is a reflection of the relative importance of advection over conduction. For the parameters used in the computations the disturbance is smallest for the low Reynolds and Marangoni number computation on the left and largest for high Reynolds and Marangoni number computation on the right. Although the wake is relatively similar in the three middle frames, the stagnation point is further away in the run on the left and the streamlines in the high Reynolds number run on the right show that although the stagnation point is close to the bubble, the fluid is pushed considerably farther down between the bubbles than in the other cases.

We next examine the interaction of two bubbles. The bubbles are released close to each other and arbitrarily oriented with respect to the temperature gradient. The initial placement is shown in Figure 2b. The domain size is two times larger in the horizontal direction than the domain for the single bubble case. The nondimensional numbers are the same as for the si-

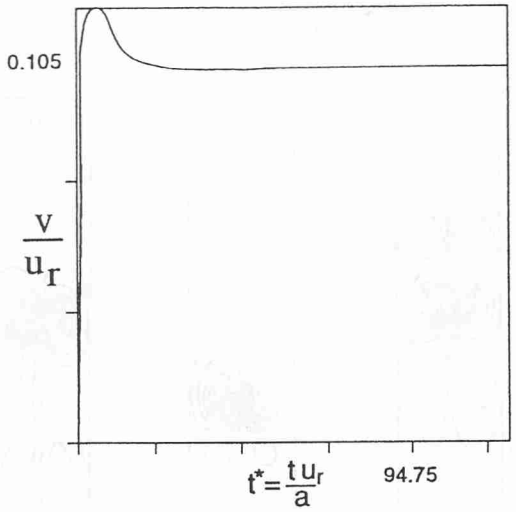

Figure 4: THE SCALED RISE VELOCITY OF THE BUBBLE IN FIGURE 3 VERSUS SCALED TIME.

gle bubble case in Figure 3. Figure 6 shows the temperature contours and the stream function contours at different time frames. As the bubbles rise, the lower bubble first catches up with the top one. It draws hot fluid down its side and as the top bubble rises, some of this fluid is drawn into its wake, thereby reducing slightly the temperature increase across the top bubble and hence its velocity. This can be seen in the streamline plot in the first frame, which is well after the motion is initiated. Once the bubbles are moving side by side, they move apart laterally, until they are equispaced across the channel (recall that the side boundaries are periodic). This is due to the fact that once the bubbles are side by side and moving upward, the outer fluid has to flow down between them to satisfy continuity. When the spacing between the bubbles is uneven there is greater flow through the larger spacings. Since the downward moving fluid is hotter, the isotherms are pushed further down where there is a large space between the bubbles than when the space is small. This is very clear in the second frame. Since the bubbles move from colder parts of the domain to the hotter ones, this leads to a lateral motion (in addition to the upward motion) where the small spaces become larger and the large spaces smaller until the bubbles have arranged themselves in a horizontal array with equal spaces between them. See the last frame. The arguments presented here are based on the uneven temperature distribution generated by the motion of the bubbles. We have not conducted these simulations for widely different parameters, but it is obvious, for example, that if the time scale of conduction was much shorter than for convection (zero Ma), then the temperature field would remain nearly undisturbed and we would expect a somewhat different behavior than observed here.

Figure 7 shows the rise velocity of each bubble for the simulation in Figure 6, as well as the velocity of the center of mass of two bubbles. The initial acceleration is similar to the one bubble case, both bubbles accelerate rapidly, reach a large velocity and then slow down. The bubble on the left that is closer to the bottom of the box, reaches a higher initial velocity and slows down more slowly than the one on the right, that was ahead initially. The left bubble therefore catches up with the right one, as seen in the previous figure, and once it does so, the right one speeds up. The bubble to the right actually obtains a velocity that is larger than the velocity of the other one and then slows down again, repeating this oscillation. Notice, that the center of mass velocity is relatively constant while the bottom bubble catches up with the top one, but then increases as the spacing between the bubbles increases.

To investigate the interaction of many bubbles, we computed the evolution of the six bubbles initially placed as shown in Figure 2c. The resolution is the same as in the two bubbles case and is approximately 25 meshes per bubble diameter. Their initial positions were selected arbitrarily. The nondimensional numbers for this case is the same as in Figure 3 and 6.

Figure 8 shows the temperature and stream function contours in the laboratory frame, at different times. We see from the plots that two bubbles separate from the rest and they rise, the separation increases further, while the others start lining up across the channel. Later on, the two leading bubbles move side by side and rise almost independent of the other bubbles. They reach a steady state velocity earlier then the other bubbles. Their motion is similar to the two bubbles interaction in Figure 6 and their terminal velocity is close to the terminal velocities of the two bubble case. Examining the velocity of each bubble in Figure 9, we see that the velocity of the center of mass of the bubbles (Figure 10a) reaches a steady state while each individual bubble does not. Especially, each bubble in the group of four bubbles has oscillating rise velocities. Also, the leading bubbles rise faster than the four bubbles left behind. The average temperature distribution at the time of the last frame is plotted in Figure 10b where the initial temperature distribution is shown by the straight

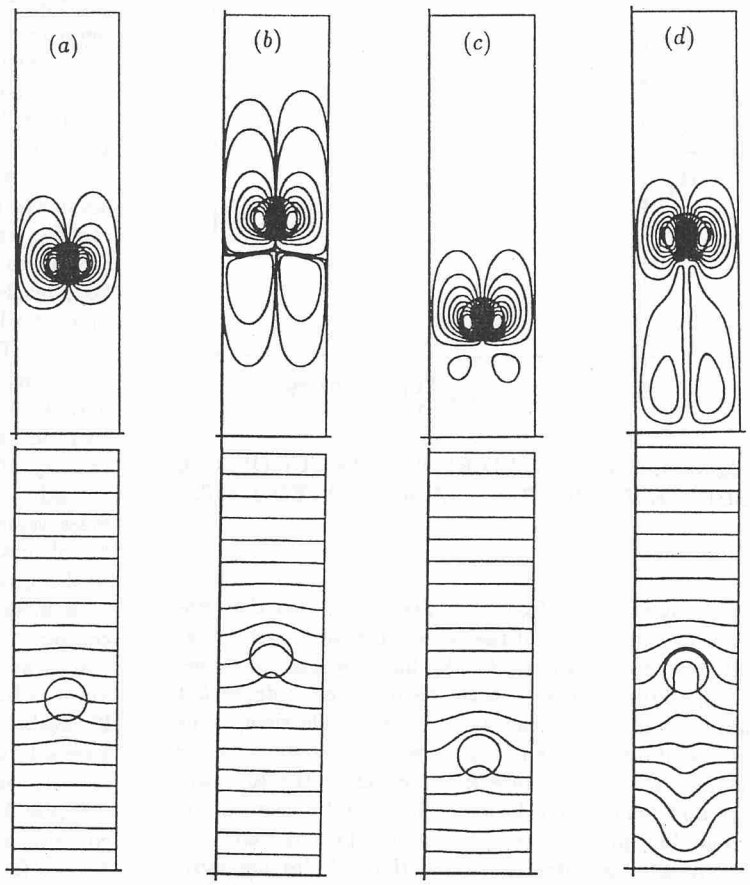

Figure 5: STEADY STATE THERMAL MIGRATION OF A SINGLE BUBBLE FOR DIFFERENT NONDIMENSIONAL NUMBERS. (*a*) $Ma = 4$, $Re = 0.2$, $\mu_i/\mu_o = 0.1$, $c_{pi}/c_{po} = 0.5$, $t^* = 22.5$ (*b*) $Ma = 20$, $Re = 5$, $\mu_i/\mu_o = 0.5$, $c_{pi}/c_{po} = 0.5$, $t^* = 62.5$ (*c*) $Ma = 40$, $Re = 0.2$, $\mu_i/\mu_o = 0.1$, $c_{pi}/c_{po} = 0.05$, $t^* = 15$ (*d*) $Ma = 400$, $Re = 2000$, $\mu_i/\mu_o = 10$, $c_{pi}/c_{po} = 0.5$, $t^* = 500$. $Ca = 0.0166$, $\rho_i/\rho_o = 0.5$ and $k_i/k_o = 0.5$ IN ALL CASES. THE INITIAL POSITION OF THE BUBBLE IS SHOWN IN FIGURE 2a. THE GRID USED HERE IS 50×200 MESHES.

line. As the bubbles rise, they perturb the initial linear temperature profile. The bubbles carry cold fluid with them upward and a warmer fluid flows back between them to conserve mass. Since the thermal capacity of the bubbles is less than the outer fluid, the net effect is to heat the region around and behind the bubbles. This is clear in Figure 10b. The temperature increases above the linear temperature profile where the two top bubbles are and even more across the bottom four bubbles. Since the temperature of the bottom wall is fixed, the gradient in the bottom region must increase, as is also seen in the close spacing of the isotherms in Figure 8.

We have computed similar interaction for four bubbles and found that for two different initial conditions they line up across the channel as they move towards the hot wall. Oscillations in their rise velocities were similar to the six bubbles case.

To investigate whether the layer formation suggested by the simulations shown above is a prominent feature in large bubble clouds, we have conducted preliminary simulations on a coarser grid where we place twenty five equal sized bubbles in a domain twice the size of the one used here. These preliminary computations suggest that while such layers may form, they will break up through instability waves many times longer than the bubble diameter. Due to the coarse resolution emploied the results may not be entirely reliable and we

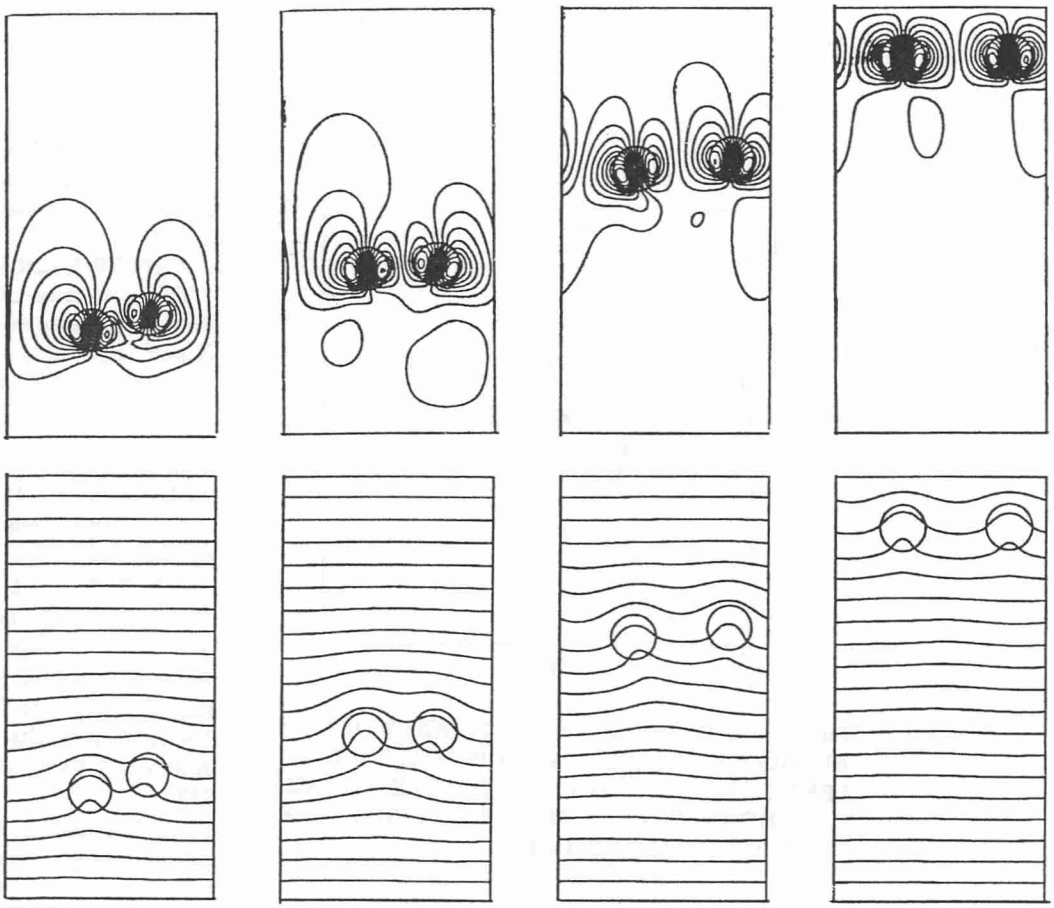

Figure 6: TEMPERATURE CONTOURS (BOTTOM) AND STREAMLINES (TOP) FOR SELECTED FRAMES FROM THE TWO BUBBLE INTERACTIONS. INITIAL CONDITIONS IN FIGURE 2b. THE NONDIMENSIONAL TIME, t^*, IS EQUAL TO 25, 50, 100, 150.

are currently conducting a more careful investigation on the behavior of large systems.

CONCLUSIONS

The major novelty of the simulations presented here is that there is no restriction on the number of bubbles simulated, the bubble shapes, nor the configuration of the bubble array. While in principle there is no limitations on the material properties simulated, we are subject to the usual requirement of high resolution for high Reynolds numbers. Furthermore, since the current version of our code is explicit, the size of the time step can become very small for very small Pr number or very large Pr when Ma number is high. These numerical restrictions put practical limitations on the range of parameters that can be simulated accurately for any given resources. The simulations presented here are, also, only two-dimensional. While this makes direct comparison of the results with experimental observations impossible, we believe that the general behavior is well predicted. The basic numerical method has been applied to three-dimensional isothermal problems (Unverdi and Tryggvason, 1992) and we anticipate that the three-dimensional counterpart of our thermal migration simulations will not pose any major problems. While we have initiated work on the three-dimensional problem, it is not completed yet. Fully three dimensional

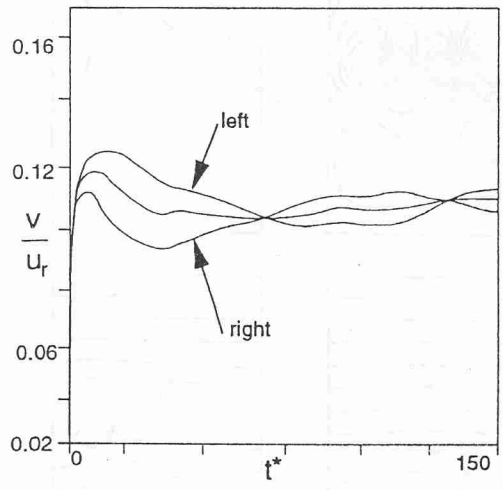

Figure 7: THE SCALED RISE VELOCITY OF THE BUBBLES IN FIGURE 6 VERSUS SCALED TIME. LEFT AND RIGHT ARE THE BUBBLE VELOCITIES, RESPECTIVELY. THE THIRD LINE IS THE CENTER OF MASS VELOCITY.

simulations will always be considerably more demanding on computational resources and we expect that we will relay heavily on two-dimensional simulations for exploratory simulations, even after the three-dimensional version is completed.

The major findings reported here is the tendency of the bubbles to line up, side by side, across the channel. While this behavior appears to be similar to what is found for spheres and cylinders in fluidized beds, where rows of spheres align themselves into a string perpendicular to the flow, the mechanism here is different. For solid spheres the reason is the low pressure region at the "waist" which attracts other particles. In the simulations here the drops actually repel each other, since cold fluid is more easily carried with the bubbles in narrow gaps than bigger ones and the bubbles generally move away from cold regions. Thus, while the bubbles line up across the channel they tend to maximize the distance between adjacent bubbles. This formation of bubble layers could be of considerable significance for, for example, material processing in microgravity where layers like these might affect the bulk properties of solidified material. We have not yet investigated the dependence of the collective behavior of bubbles on the various nondimensional numbers, but expect to do so in the near future, We also intend to conduct larger scale simulations and to investigate the stability of a bubble layer to long wavelength disturbances.

ACKNOWLEDGMENTS

This work is supported by NASA grant NAG3-1317. Some of the computations were done at the San Diego Supercomputing Center which is funded by the National Science Foundation.

REFERENCES

Anderson, J. L., 1985, "Droplet Interaction in Thermocapillary Motion," *Int. J. Multiphase Flow*, vol. 11, pp. 813-824.

Ascoli, E. P. and Leal, L. G., 1990, "Thermocapillary Motion of a Deformable Drop Toward a Planar Wall," *J. Colloid Interface Sci.*, vol. 138, pp. 220-230.

Balasubramaniam, R. and Lavery, J. E., 1989, "Numerical Simulation of Thermocapillary Bubble Migration Under Microgravity for Large Reynolds and Marangoni Numbers," *Num. Heat Transfer A*, vol. 16, pp. 175-187.

Balasubramaniam, R. and Chai, A., 1987, "Ther capillary Migration of Droplets: An Exact Solutio. Small Marangoni Numbers," *J. Colloid Interface Sci.*, vol. 119, pp. 531-538

Barton, K. D. and Subramanian, R. S., 1989, "The Migration of Liquid Drops in a Vertical Temperature Gradient," *J. Colloid Interface Sci.*, vol. 133, pp. 211-222.

Chen, J. C. and Lee, Y. T., 1992, "Effect of Surface Deformation on Thermocapillary Bubble Migration," *AIAA J.*, vol. 30, pp. 993-998.

Clift, R., Grace, J. R. and Weber, M. E., 1978, *Bubbles, Drops, and Particles*, Academic Press.

Dill, L. H. and Balasubramaniam, R., 1988, "Unsteady Thermocapillary Migration of Bubbles," *NASA Technical Memorandum 101338*, NASA Lewis Research Center.

Merrit, R. M. and Subramanian, R. S., 1988, "The Migration of Isolated Gas Bubble in a Vertical Temperature Gradient," *J. Colloid Interface Sci.*, vol. 125, pp. 333-339.

Meyyapan, M. and Subramanian, R. S., 1984, "The Thermocapillary Motion of Two Bubbles Oriented Arbitrarily Relative to a Thermal Gradient," *J. Colloid Interface Sci.*, vol. 97, pp. 291-294.

Meyyapan, M. and Subramanian, R. S., 1987, "Thermocapillary Migration of a Gas Bubble in an Arbitrary Direction with Respect to a Planar Surface," *J. Colloid Interface Sci.*, vol. 115, pp. 206-219.

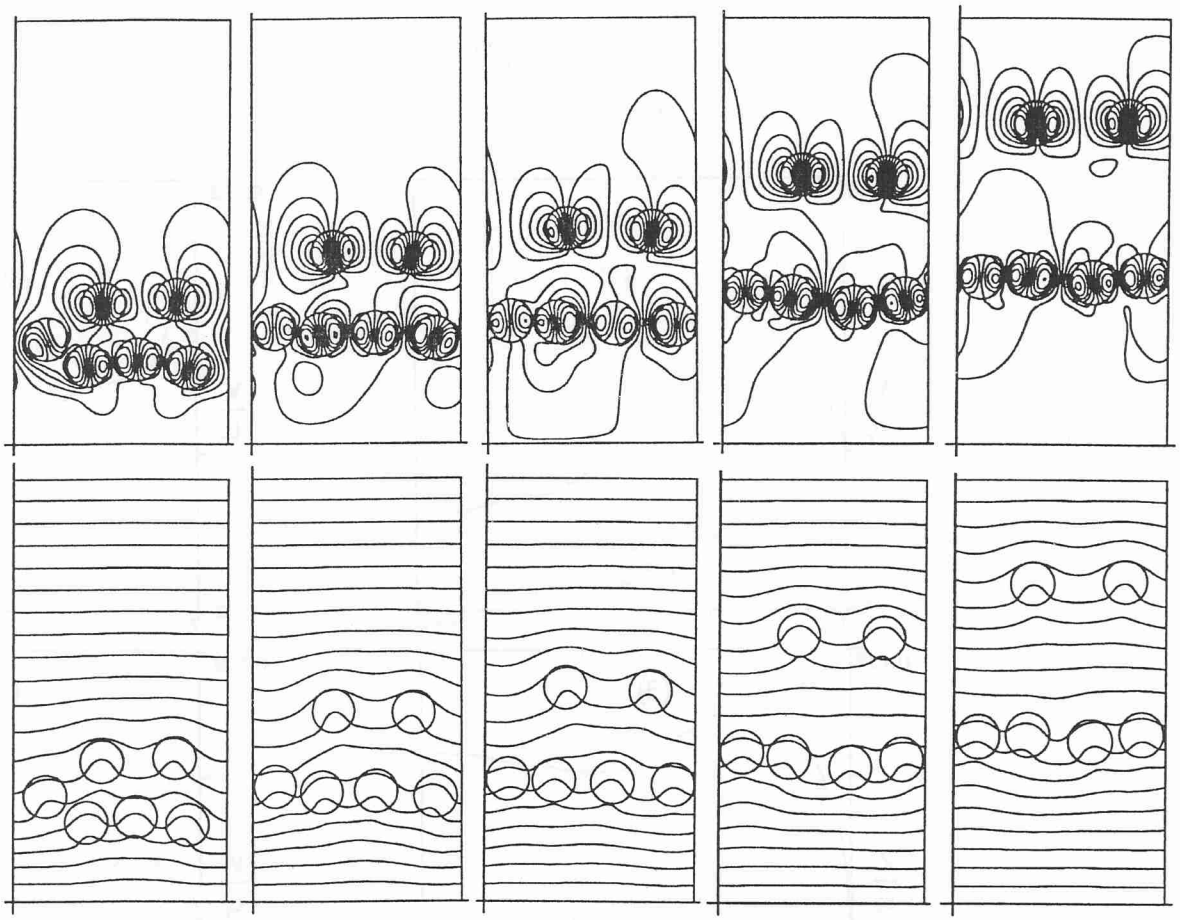

Figure 8: TEMPERATURE CONTOURS (BOTTOM) AND STREAMLINES (TOP) FOR SELECTED FRAMES FROM THE COMPUTATION OF SIX BUBBLE INTERACTIONS. INITIAL CONDITIONS IN FIGURE 2c. THE NONDIMENSIONAL TIME, t*, IS EQUAL TO 20, 40, 50, 75, 100.

Peskin, C. S., 1977, "Numerical Analysis of Blood Flow in the Heart," *J. Comput. Phys.*, vol. 25, pp. 220-252.

Shankar, N. and Subramanian, R. S., 1988, "The Stokes Motion of a Gas Bubble Due to Interfacial Tension Gradients at Low to Moderate Marangoni Numbers," *J. Colloid Interface Sci.*, vol. 123, pp. 512-522.

Strape, J. V., 1992, "Interactions and Collisions of Bubbles in Thermocapillary Motion," *Phys. of Fluid*, vol. A 4, pp. 1883-1900.

Subramanian, R. S., 1981, "Slow Migration of a Gas Bubble in a Thermal Gradient," *AIChE J.*, vol. 27, pp. 646-654.

Subramanian, R. S., 1992, "The Motion of Bubbles and Drops in Reduced Gravity," *Transport Processes in Bubbles, Drops and Particles*, Chhabra, R. P. and De Kee, D., ed., Hemisphere Publishing Corp., Washington, D.C., pp. 1-42.

Thompson, R. L., Dewitt, K. J. and Labus, T. L., 1980, "Marangoni Bubble Motion Phenomenon in Zero Gravity," *Chem. Eng. Commun.*, vol. 5, pp. 299-314.

Trefethen, L. M., 1963, *Surface Tension in Fluid Mechanics*, a color film by Encyclopedia Brittanica Educational Cooporation, Film No. 21610.

Unverdi, S. O., 1990, *Ph.D. Thesis*, The University of Michigan, Ann Arbor, MI.

Unverdi, S.O. and Tryggvason, G., 1992, "A Front Tracking Method for Viscous Incompressible Flows," *J. Comput. Phys.*, vol. 100, pp. 25-37.

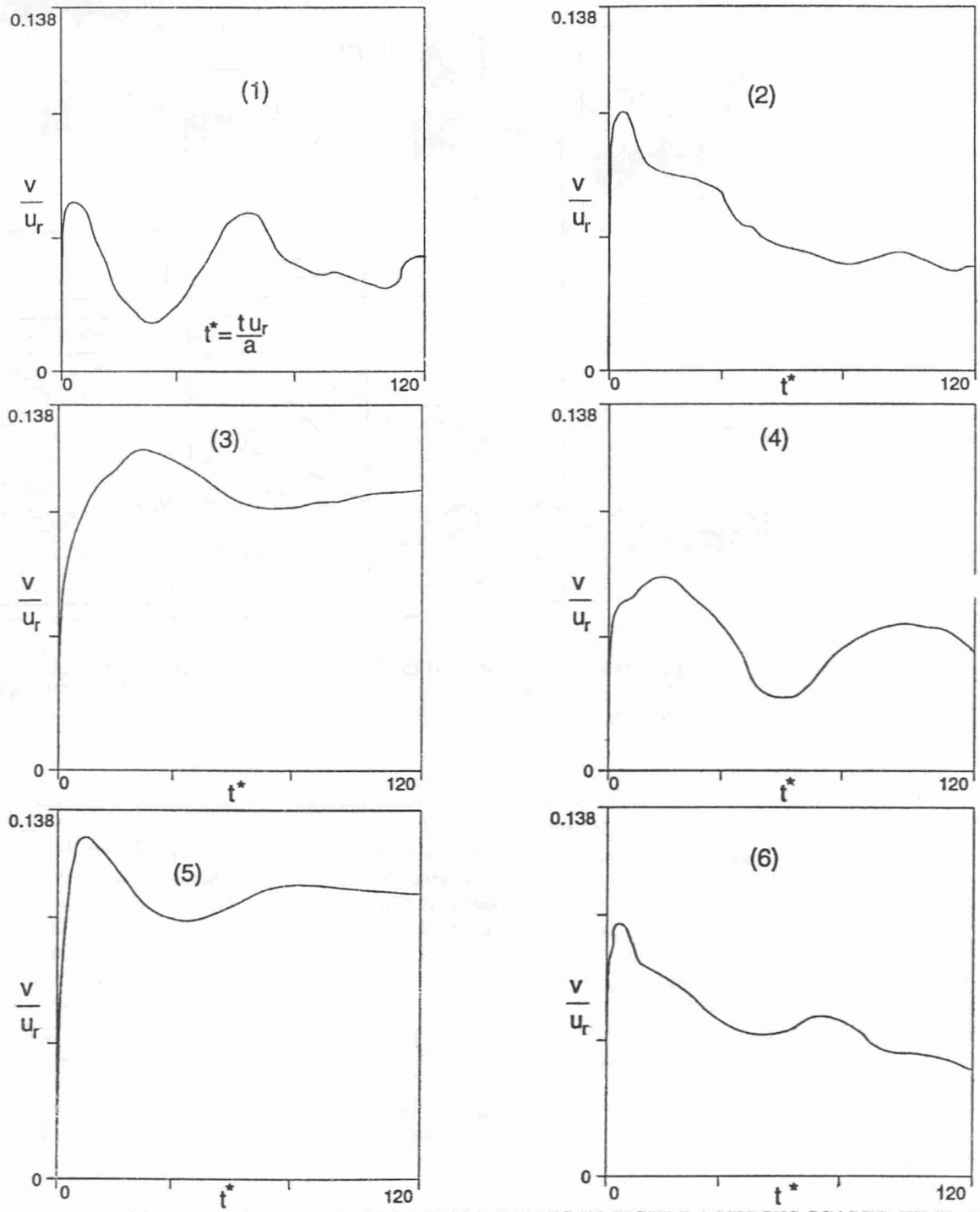

Figure 9: THE SCALED RISE VELOCITY OF THE BUBBLES IN FIGURE 8 VERSUS SCALED TIME. THE BUBBLES ARE NUMBERED FROM LEFT TO RIGHT.

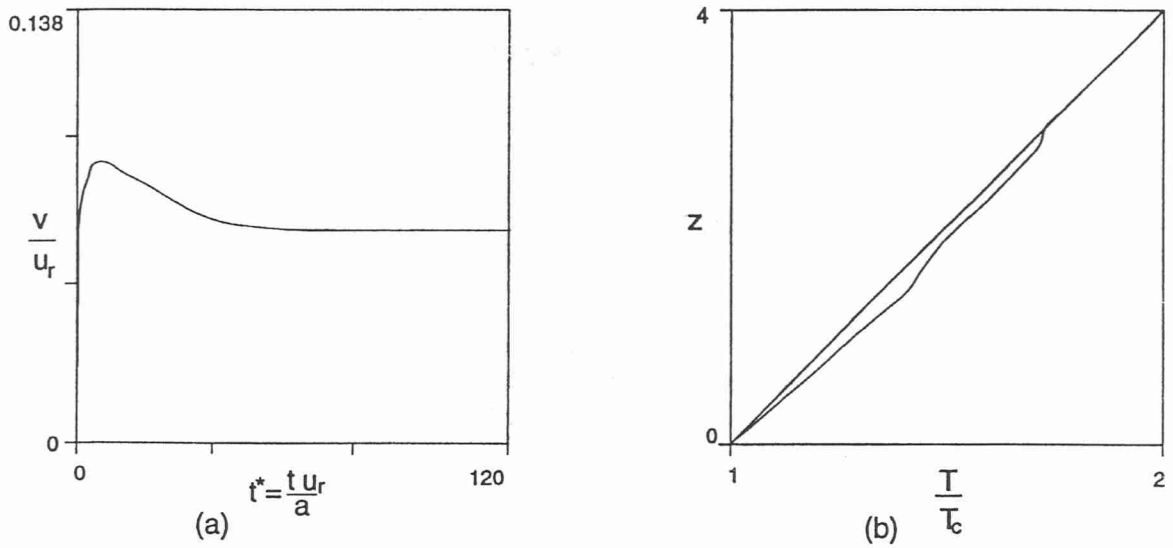

Figure 10: (*a*) THE SCALED RISE VELOCITY OF THE CENTER OF MASS OF THE BUBBLES IN FIGURE 8 VERSUS SCALED TIME. (*b*) THE AVERAGE SCALED TEMPERATURE VERSUS VERTICAL DIRECTION FOR THE LAST FRAME IN FIGURE 8. NOTE THAT STRAIGHT LINE IS INITIAL TEMPERATURE DISTRIBUTION.

Unverdi, S. O. and Tryggvason, G., 1992, "Computations of Multi-fluid Flows," *Physica D*, vol. 60, pp. 70-83.

Wozniak, G. and Siekmann, J., 1989, "Experimental Investigation of Thermocapillary Droplet Motion in Reduced Gravity - Two Sounding Rocket Experiments," *Appl. Microgravity Tech.*, vol. 2, pp. 173-175.

Young, N. O., Goldstein, J. S. and Block, M. J., 1959, "The Motion of Bubbles in a Vertical Temperature Gradient," *J. Fluid Mech.*, vol. 6, pp. 350-356.